NONLINEAR ALUMINUM NITRIDE PHOTONIC CRYSTAL MEASUREMENT USING TAPERED FIBER

BY

WORAPRACH KUSOLTHOSSAKUL

THESIS

Submitted in partial fulfillment of the requirements
for the degree of Master of Science in Electrical and Computer Engineering
in the Graduate College of the
University of Illinois at Urbana-Champaign, 2019

Urbana, Illinois

Adviser:

Assistant Professor Kejie Fang

ABSTRACT

Second harmonic generation is a nonlinear optical process that is an important bridge in the conversion between infrared and visible light. A ring resonator with a top layer of aluminum nitride, a material with high second order susceptibility, can achieve an efficient coupling between 780 nm visible light and 1550 nm infrared light. A tapered region is also integrated to improve the light transmission between an optical fiber and an on-chip waveguide. We demonstrate the high value of nonlinear coupling interaction strength, the phase matching of the mode extraction from the waveguide to the ring resonator, and the fabrication of tapered optical fiber and tapered aluminum nitride waveguide.

ACKNOWLEDGMENTS

I would first like to thank my advisor Professor Kejie Fang for overseeing and supporting my master's education. His advice has been a great help. I also would like to thank Edmond Chow, Lavendra Mandyam, and staff in the Micro and Nanotechnology Laboratory for teaching and facilitating me with cleanroom fabrication. Their assistance is greatly appreciated. I would also like to thank Mengdi Zhao, Tao Hong, and everyone in Professor Fang's research group for their cooperation and feedback on this work.

TABLE OF CONTENTS

CHAPTER 1

INTRODUCTION

Telecommunication normally employs an infrared wavelength in an optical fiber connection to transfer information [1,2]. The optical fiber has a low absorption of the light between 1.3 and 1.6 μm. Therefore, we can use this range of signal to send data over a long distance due to the low loss. Additionally, there is an erbium doped fiber amplifier, which has a high gain in the infrared regime. This fiber amplifier can consequently pump up an infrared signal. These are the advantages of infrared signal in an optical fiber system. However, the infrared spectrum has a low energy bandgap and is therefore difficult to utilize in an on-chip semiconductor device. Higher frequency signals, including visible light and microwaves, are preferred for their higher bandgap. There is a mismatch between fiber communication and semiconductor wavelength.

Aluminum nitride is a material with a high $\chi^{(2)}$ nonlinear factor. This material property offers an application in second harmonic generation [1], which is the phenomenon in which two photons with the same frequency combine in a nonlinear material and generate a new photon with frequency twice and wavelength half of the original photons. We can utilize the second harmonic generation to convert between 780 nm wavelength visible light and 1550 nm wavelength infrared light, which is frequently used in communication. The ring resonator is the geometry that can improve this nonlinear process [2,3].

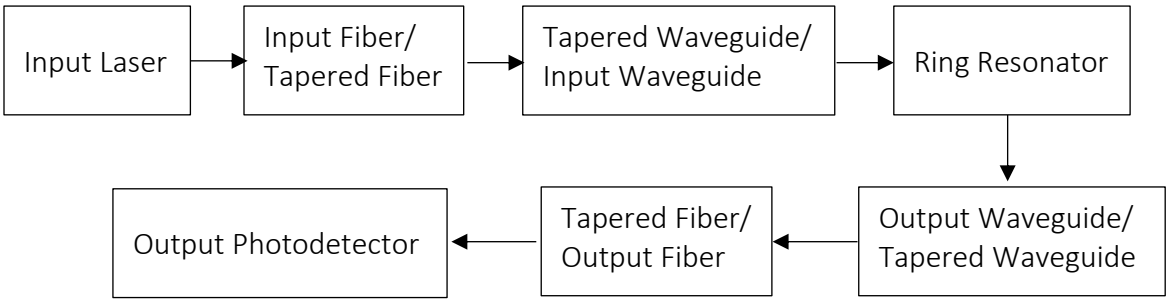

Figure 1.1: Wavelength Conversion Block Diagram

The light input from the laser travels through the optical fiber and then couples to an on-chip waveguide, as shown in figure 1.1. The optical fiber geometry affects the light transmission between the fiber and the waveguide. An adiabatic tapered region is a promising device to efficiently transfer light between fiber and waveguide [4,5]. An optical fiber and a waveguide will have a gradually decreasing radius, forming a taper. The overlapping interface between two tapered regions will lead to superior light coupling [6]. The signal also couples from the waveguide into the ring resonator. The ring then converts from 1550 nm infrared to 780 nm visible light or vise versa. The converted light then couples out to the waveguide and then to the output optical fiber for measurement.

This thesis reports work using a silicon substrate with a 1 μm thick layer of thermal silicon oxide and a 600 nm thick layer of aluminum nitride deposited on top. The aluminum nitride is patterned using an electron beam lithography and dry etch machine because of the small feature size. The patterned aluminum nitride will be a tapered waveguide with a photonic crystal hole, which has a bandgap that matches the input light wavelength and will reflect the same wavelength of light back. The photonic crystal is first used instead of the ring resonator to test the coupling efficiency between the tapered fiber and the tapered waveguide.

CHAPTER 2

COMPUTATIONAL SIMULATION

2.1 Nonlinear Coupling Interaction Strength

The ring resonator can be described by a Hamiltonian equation, $\mathcal{H} = \omega_b b^\dagger b + \omega_c c^\dagger c + Gcb^\dagger e^{-i\omega_a t} + G^* c^\dagger b e^{i\omega_a t}$ where $G = \langle a \rangle g$ [2]. The terms $a, b,$ and c are annihilation operators of three frequency modes in the ring while $b^\dagger$ and $c^\dagger$ are generation operators of two modes. g represents a nonlinear coupling interaction strength whereas $\langle a \rangle$ is a mean photon number of mode a, which is strongly pumped by a resonance laser at frequency ω_a. The value of g can be calculated by the $\chi^{(2)}$ coefficient, and the field inside the ring, $g_{NL} = \omega_a \sqrt{\omega_b} \frac{\int \varepsilon_0 \chi^{(2)}_{zzz} (E^*_{az})^2 E_{bz}\, dV}{\int \varepsilon (|E_a|^2\, dV * \sqrt{\int \varepsilon (|E_b|^2\, dV}}$.

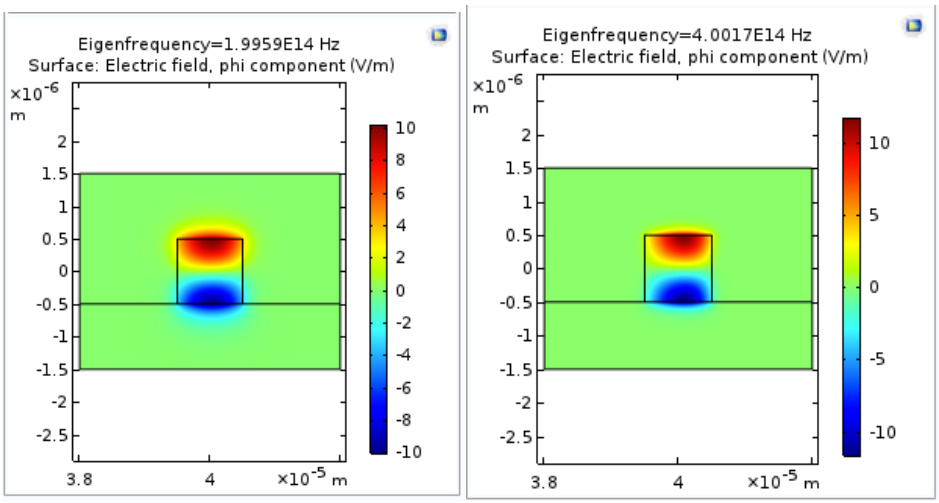

Figure 2.1: TM Mode Azimuthal Electric Field inside Ring Cross Section

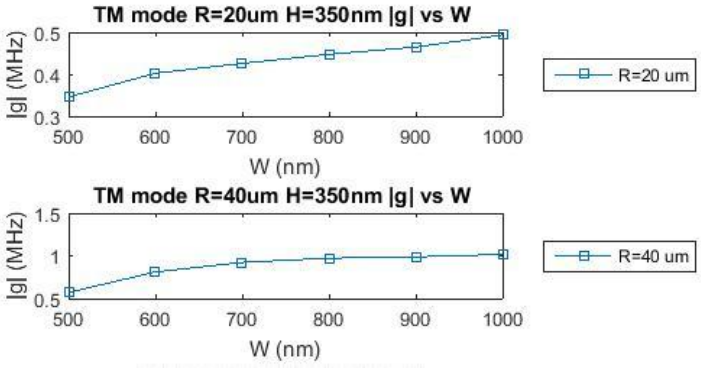

Figure 2.2: $|g|$ vs. W of 350 nm Thick Rings with 20 μm and 40 μm Radius

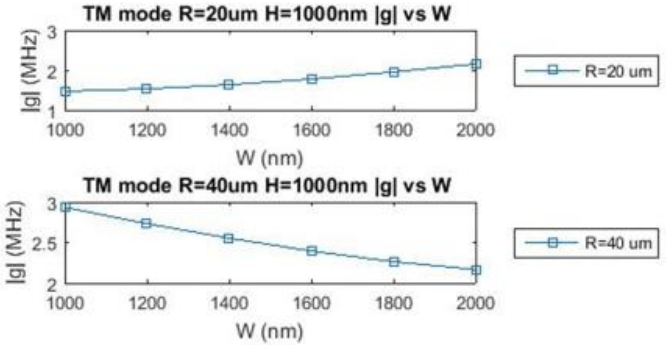

Figure 2.3: $|g|$ vs. W of 1 μm Thick Rings with 20 μm and 40 μm Radius

The program Comsol is used to simulate the nonlinear interaction strength. We create a simulation varying ring thickness, width, and radius at two frequencies, $\omega_a = \omega_c = 2\pi \times 2$ THz (1.5 μm) and $\omega_b = 2\pi \times 4$ THZ (780 nm), with both TE and TM modes. Figure 2.1 shows the azimuthal electric field strength in a cross section of the ring with 1 μm thickness, 1 μm width and 40 μm radius at two different frequencies. Figures 2.2 and 2.3 are graphs representing the relation between the nonlinear coupling strength, g, and the width of the 350 nm and 1 μm thick ring resonators. The g value from TE modes, which is around 40 to 1000 Hz, is significantly smaller than TM mode, which is approximately 1 to 3 MHz. The TM mode result shows a noteworthy value, which offers a strong conversion between two frequency modes.

2.2 Phase Matching Mode Extraction

Using the Lumerical program, we simulate the transmission and the mode inside the waveguide and the ring resonator. The TM0 780 nm light input is from the laser through an optical fiber with a tapered tip and transfers to the waveguide. The light inside the waveguide has to evanescently couple to the ring resonator. This leads to the higher mode inside the ring resonator [1]. The TM2 780 nm light is found inside the ring. We use a wraparound waveguide so we ignore the curvature of the ring resonator in the simulation, as shown in figure 2.4.

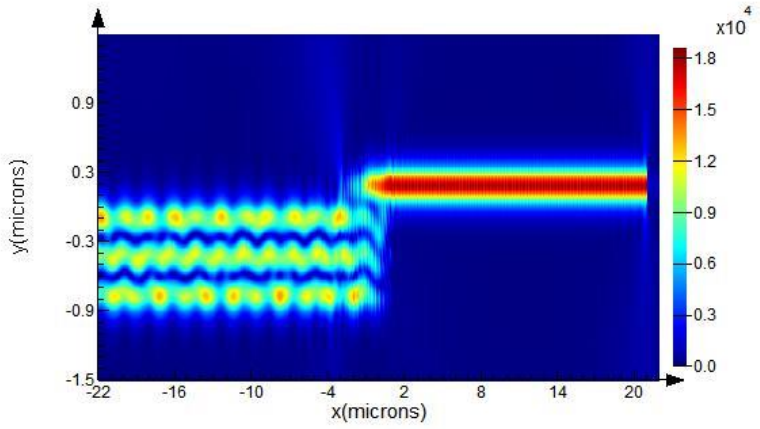

Figure 2.4: Intensity Profile of Light in Evanescent Coupling Region

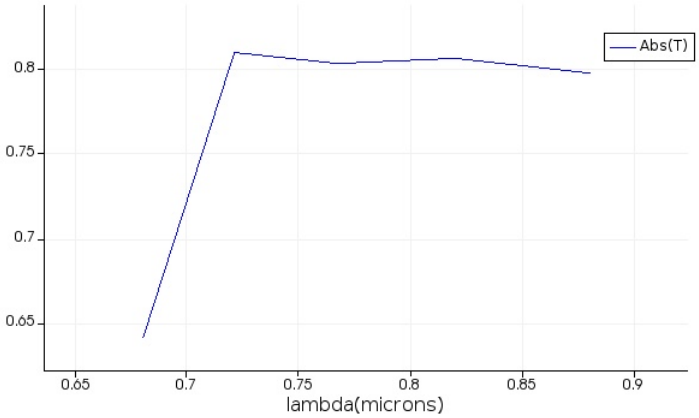

Figure 2.5: Transmission through Ring Resonator

We try to maximize the coupling efficiency by optimizing phase matching, which creates the same effective index inside both the waveguide and the ring, reducing the reflection and loss of the light. The ring resonator has 843 nm width and TM2 effective

index of 1.6944. We found that the waveguide with 190 nm width has TM0 effective index of 1.6936, which is phase matched to the ring resonator. Figure 2.4 is a model with 100 nm ring and waveguide gap, and 3.92 μm coupling length. The result of the simulation, figure 2.5, shows that we can achieve good transmission of the TM0 780 nm mode input to TM2 780 nm mode in the ring resonator.

CHAPTER 3

TAPERED ALUMINUM NITRIDE FABRICATION

In order to integrate a semiconductor device to an optical fiber network, a coupling region between the on-chip waveguide and the optical fiber is required. However, the coupling between the chip and the optical fiber would cause some transmission loss during the discontinuity. There are multiple coupling methods such as butt-coupling, where the core of the fiber is connected to the waveguide, and grating coupling, where the light from the fiber propagates into an on-chip diffraction grating before the waveguide [7]. These two approaches have theoretically less than 80 percent coupling efficiency. A new coupling method with a coupling efficiency of 95 percent uses a tapered coupling region [8]. This coupling utilizes an adiabatic mode transformation, $\frac{dn_{wg}}{dx} < \left(\frac{2\pi}{\lambda}\right)\left|n_{eff,1}(x) - n_{eff,2}(x)\right|^2$ [6]. The term n_{wg} is an effective index of the waveguide while $n_{eff,1}$ and $n_{eff,2}$ are the effective indices of the first and second modes inside a tapered waveguide. The gradual change of radius along the taper confines the optical power in a single eigenmode, thereby reducing the energy loss into other eigenmodes.

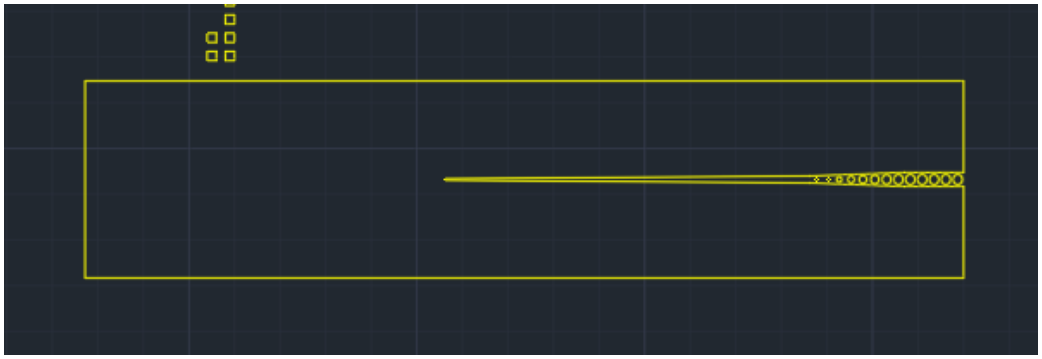

Figure 3.1: The Diagram of a Tapered Waveguide

In order to satisfy the adiabatic condition and maximize coupling efficiency, a tapered waveguide needs to have a half angle approximately 2°. The taper tip size is 100 nm while the taper length is 24 μm. Theoretically, a sharp tip is more desirable but it is difficult to achieve with the etching process during fabrication. Figure 3.1 shows the diagram of the tapered waveguide. At the end of the taper, there is a photonic crystal that is designed to reflect 1.5 μm light back out. The photonic crystal is an elliptical hole with width of 550 nm and height of 500 nm in a unit cell size of 650 nm while the waveguide width is 780 nm. These patterned holes will cause aluminum nitride to have an energy gap of 0.826 eV. When the light is transmitted along the waveguide and reaches the photonic crystal regions, an electron will move from a valence band to a conduction band. When an electron retreats back to valence band, it emits light that matches the energy gap, which is 1.5 μm in wavelength. The photonic hole also is tapered to accommodate a transition of the waveguide radius change.

The silicon chip with aluminum nitride layer on thermal oxide is patterned by using an electron beam machine. We use ZEP520A, an electron beam resist, to create a mask for the aluminum nitride. After exposing to the electron beam by JEOL JBX-6000FS electron beam lithography system at 50 kV, the substrate is then etched by inductively coupled plasma - reactive ion etching (ICP-RIE). However, the etch rate of ZEP520A is significantly faster than that of aluminum nitride. The silicon dioxide is introduced as a hard mask between aluminum nitride and ZEP520A.

We first deposit silicon dioxide on top of the aluminum nitride layer using plasma-enhanced chemical vapor deposition. Then, after the substrate is spin-coated with ZEP520A and exposed to electron beam, we use ICP-RIE silicon dioxide etch recipe, which completely etches the top layer of ZEP520A. The silicon dioxide layer will retain the pattern. We next use the ICP-RIE aluminum nitride recipe to etch the silicon dioxide mask and pattern the aluminum nitride. The selectivity of ZEP520A to silicon dioxide is 1.4:1 and the selectivity of silicon dioxide to aluminum nitride is 1:1.57. In order to etch 600 nm of aluminum nitride, we use 120 nm silicon dioxide and 550 nm ZEP520A. Lastly, the aluminum nitride tapered region has to be detached from the thermal silicon dioxide layer underneath to minimize leakage when coupling to a tapered fiber. We use 10:1 buffered oxide etch solution for 30 minutes to partially dissolve the thermal oxide

layer under the tapered aluminum nitride. This etching step releases the tapered waveguide from the substrate, allowing contact of the tapered fiber and the aluminum nitride waveguide.

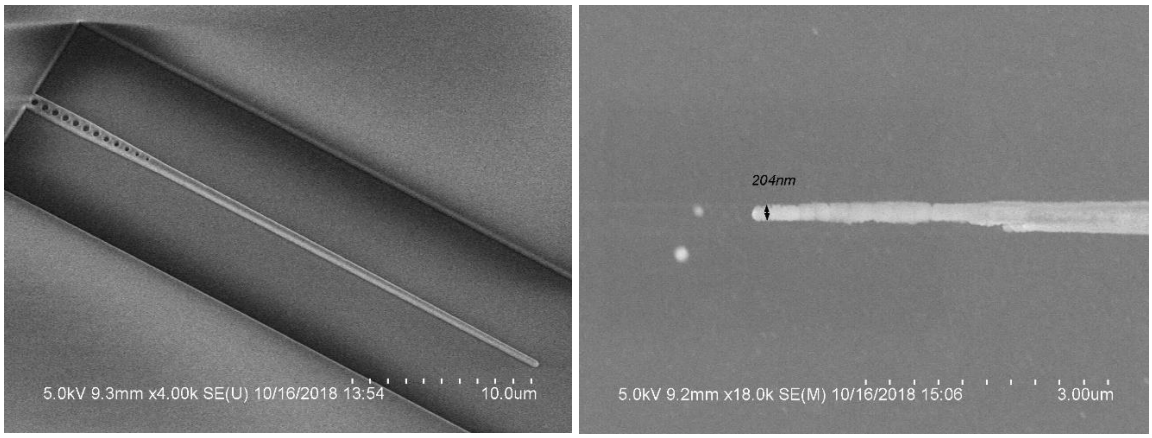

Figure 3.2: The Tapered Aluminum Nitride SEM Image

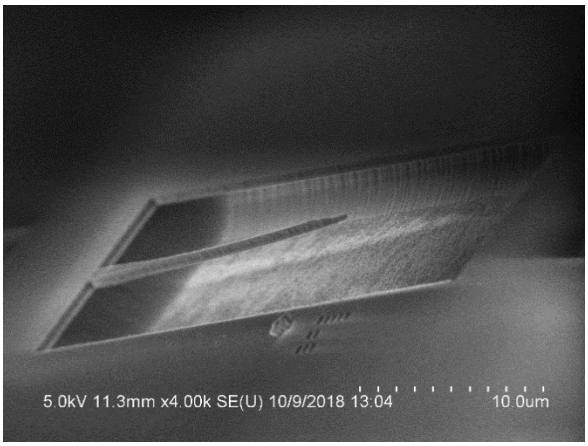

Figure 3.3: The Released Tapered Waveguide

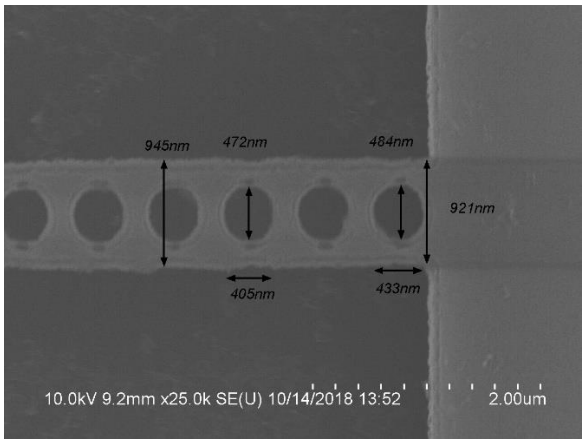

Figure 3.4: The Photonic Crystal

Figures 3.2 and 3.3 show the resulting tapered aluminum nitride waveguide that is released from the thermal oxide layer. However, the tip of the taper is shortened and slightly deformed. The tip, which is 200 nm in diameter, is larger than the electron beam exposure dimension, which is 100 nm. This problem may arise from an electron beam proximity effect, by which the incident electron backscatters and alters the pattern dimension, or from the plasma in the ICP-RIE recipes overetching the sub-100 nm feature. Furthermore, the waveguide width is larger than expected. The initial pattern is 780 nm while the result in figure 3.4 is 945 nm. The photonic crystal holes also have shrunk; the diameter is approximately 100 nm smaller than the design. The taper tip size discrepancy may lead to lower coupling efficiency while the waveguide width and photonic hole size may reflect back a different wavelength of light.

CHAPTER 4

TAPERED FIBER FABRICATION

The tapered fiber that is used for the ring resonator measurement is manufactured from an optical fiber. The typical optical fiber, starting from the center, consists of a core, a cladding, and a coating. The core material is surrounded by a cladding material with lower refractive index. Snell's law explains the relationship between the incident angle, θ_1, and the refraction angle, θ_2, of waves at an interface of two media: $n_1 \sin\theta_1 = n_2 \sin\theta_2$. When the light travels from a higher refractive index medium to a lower index medium, there is a range of incident angle where the light is completely reflected back at the media boundary. By virtue of this total internal reflection phenomenon, the optical fiber can carry light along its length. The light will always reflect at the core and cladding interface, keeping it inside the core region. In addition, the plastic coating encloses the cladding only to act as a protection. Both 780 nm and 1550 nm single-mode optical fibers have approximately 250 μm diameter in total, while the total cladding and core diameter is 125 μm.

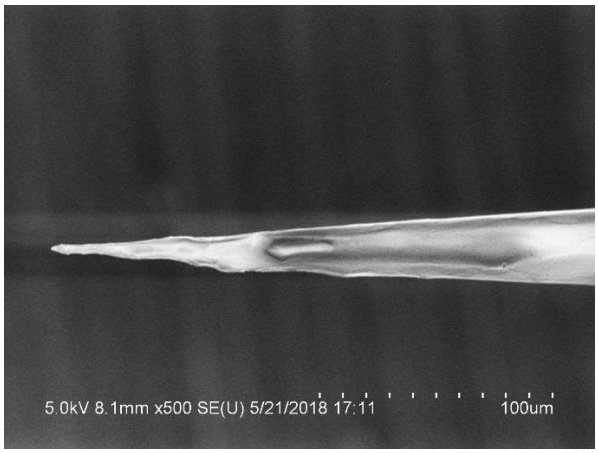

Figure 4.1: The Taper Fiber Tip Image

Because the plastic coating only provides structural stability to the fiber and does not affect the total internal reflection inside the fiber core, the coating is first stripped and removed from the fiber. The cladding and core parts of the fiber are made of glass. We can create a tapered fiber by using hydrofluoric acid, which dissolves glass. To create a taper, the fiber is then drawn out of the hydrofluoric acid at a constant speed using a motorized stage control [4,9]. The fiber in figure 4.1 exhibits a rough fiber surface, which may be the result of a dirty fiber or of the meniscus effect at the hydrofluoric acid surface. The curvature of the acid from the surface tension leads to uneven etching when pulling out the fiber.

Before etching a fiber in hydrofluoric acid, a piranha cleaning is used to clean the fiber. The stripped fiber tip is dipped into piranha solution, a combination of 3 parts sulfuric acid and 1 part hydrogen peroxide that is used to clean organic material from the substrate. It can remove any dust particles attached to the fiber surface that may cause an uneven gradual taper formation during an etching step. Importantly, the o-xylene oil is added to the hydrofluoric surface to prevent the evaporation of the acid, and the meniscus effect occurs at the top surface of the fiber [4,10], which may cause an irregular fiber exterior.

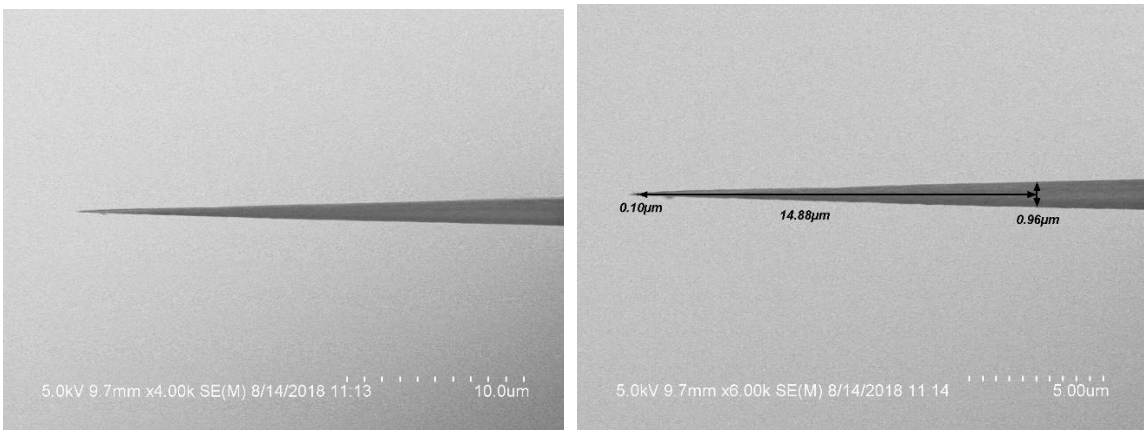

Figure 4.2: The Tapered Tip Image Formed in an Acid with O-xylene

The resulting fiber shown in figure 4.2 was drawn out of 49% hydrofluoric acid in 37.5 minutes; the fiber is moving upward at 1.909 μm/s. We can achieve a tapered fiber with a tip smaller than 100 nm, and the half taper angle is between 1.5° and 2°. These specifications should offer an excellent light coupler between the fiber and the waveguide. The taper angle, θ_t, can be adjusted by changing the withdrawal speed, v, of the fiber from the acid. The etch rate of glass in 49% hydrofluoric acid, R, is approximately 1.667 μm per minute. The relation of the taper angle and the stage control speed is $\tan\theta_t = \frac{R}{v}$.

CHAPTER 5

DISCUSSION

5.1 Conclusion

We demonstrated that the aluminum nitride ring resonator has a high TM mode nonlinear coupling interaction strength, which shows a promising wavelength conversion, and the phase matching of the 780 nm waveguide and ring resonator can enable a good transmission of light and energy from TM0 mode to TM2 mode. We successfully fabricated a tapered fiber using a motorized stage control in hydrofluoric acid with o-xylene oil top layer. The tapered fiber result has a tip smaller than 100 nm in diameter and half taper angle between 1.5° and 2°. We also created a tapered waveguide from aluminum nitride substrate. The tapered waveguide is detached from the oxide underneath, but the tip shape is not smooth and the tip size is larger than desired.

5.2 Future Work

Due to the fabrication problem discussed in Chapter 3, we cannot create a tapered waveguide with a tip smaller than 200 nm diameter. By adjusting the electron beam lithography and dry etching recipe, we may achieve a finely tapered waveguide that will match the tapered fiber, enabling a high transmission from the optical fiber to the on-chip waveguide. With this done, we can then add the ring resonator to measure the second harmonic conversion efficiency of the ring resonator from the aluminum nitride material.

REFERENCES

[1] Bruch, A. W., Liu, X., Guo, X., Surya, J. B., Gong, Z., Zhang, L., and Tang, H. X. "17000%/W second-harmonic conversion efficiency in single-crystalline aluminum nitride microresonators." *Applied Physics Letters, 113(13)* (2018).

[2] Guo, X., C.-L. Zou, H. Jung, and H.X. Tang. "On-chip strong coupling and efficient frequency conversion between telecom and visible optical modes." *Physical Review Letters, 117 (12)* (2016).

[3] Zhang, M., Wang, C., Cheng, R., Shams-Ansari, A., and Lončar, M. "Monolithic ultra-high-Q lithium niobate microring resonator." *Optica 4*, 1536-1537 (2017).

[4] Rickelt, L. F., Kühl, M., and Ottosen, L. D. M. "Etching of multimode optical glass fibers: A new method for shaping the measuring tip and immobilization of indicator dyes in recessed fiber-optic microprobes." *Sensors and Actuators, B: Chemical, 211,* 462–468 (2015).

[5] Chenari, Z., Latifi, H., Ghamari, S., Hashemi, R. S., and Doroodmand, F. "Adiabatic tapered optical fiber fabrication in two step etching." *Optics and Laser Technology, 76*, 91–95 (2016).

[6] Burek, M. J., Meuwly, C., Meesala, S., Lončar, M., Evans, R. E., Bhaskar, M. K., and Bielejec, E. "Fiber-coupled diamond quantum nanophotonic interface." *Physical Review Applied*, 8(2) (2016).

[7] Chen, X., Li, C., & Tsang, H. K. "Device engineering for silicon photonics." *NPG Asia Materials, 3(1),* 34–40. (2011).

[8] Tiecke, T. G., Nayak, K. P., Thompson, J. D., Peyronel, T., De Leon, N. P., Lukin, M. D., & Vuletić, V. "Efficient fiber-optical interface for nanophotonic devices." *Optica, 2(2),* 70–75. (2015).

[9] Abdul Rashid, A. R., Nasution, A. A., Suranin, A. H., Taib, N. A., Mukhtar, W. M., Dasuki, K. A., and Ehsan, A. A. "Chemical tapering of polymer optical fiber." *EPJ Web of Conferences, 162*, 1–5 (2017).

[10] Takahashi, K.M. "Meniscus shapes on small diameter fibers." *Journal of Colloid and Interface Science 134 (1),* 181–87 (1989).